International Journal of Intelligent Robotics and Applications (2020) 4:136–148
https://doi.org/10.1007/s41315-020-00133-4

REGULAR PAPER

Worst case identification based topology optimization of a 2-DoF hybrid robotic arm

Zenghui Chong[1] · **Fugui Xie**[1,2] · **Xin-Jun Liu**[1,2] · **Jinsong Wang**[1] · **Peng Li**[1]

Received: 28 November 2019 / Accepted: 23 April 2020 / Published online: 5 May 2020

Abstract

In the design of robotic arms, structural topology optimization considering variable configurations with high computational efficiency is still a challenging issue. In this paper, the worst case identification based topology optimization of a 2-DoF hybrid robotic arm is accomplished, and the presented work mainly covers: (1) efficient worst case identification; (2) optimization problem construction and (3) iterative criterion and filtering method with fast convergence. The forward kinematics are investigated to identify the workspace. Thereafter, the equivalent external load is proposed to unify the effect of axial load and shear by force analysis and compliance calculation. The worst case is the load case with maximum compliance and can be located efficiently by searching for the maximum equivalent external load. The optimization problem is constructed based on the solid isotropic material with penalization (SIMP) interpolation scheme. For links with multiple worst cases, the objective function is constructed as the weighted sum of compliance under each worst case. For better computational efficiency, the modified guide-weight method is used to solve the optimization problem. To eliminate the mesh dependence and checkerboard problem, a guide weight filtering method is proposed. Under the guidance of derived optimal topology, the CAD model of the hybrid robotic arm is presented. The effect of the optimization is testified through performance comparison in finite element analysis. The optimization method can derive the optimal topology with global validity within allowable computational time and the optimization approach can be applied to other hybrid robotic arms as well.

Keywords Worst case identification · Hybrid robotic arm · Topology optimization · Modified guide-weight method

1 Introduction

A 2-DoF hybrid robotic arm is developed based on a planar hybrid mechanism in Ref. (Liu et al. 2015). In industry, robots based on parallel or hybrid mechanisms have been widely used because of their advantages like low inertia, high stiffness and quick dynamic response (Xie et al. 2015; Bi et al. 2019). Many efforts have also been devoted to their theoretical analysis as well (Luo et al. 2019; Chen et al. 2015). In the development of a hybrid robot, the structure influences the performance greatly from the aspect of stiffness, inertia, dynamic performance, and etc. (Jin et al. 2018). Since the robotic arm has time-varying kinematic configurations and joint forces during its motion, optimization for a single load case or several load cases cannot guarantee global validity. In addition, the computational expense is normally high for the optimization of a hybrid robotic arm, how to reduce computational time is still challenging (Wang et al. 2019). Therefore, the topology optimization of the 2-DoF hybrid robotic arm with global validity and high computational efficiency is worth investigating.

Since time-varying configurations influence the load cases of each link in the workspace, the topology optimization of the robotic arm is more complicated than topology optimization of structures under static or vibrating loads (Smyl 2018). Early studies mainly optimize the structure of robotic arms for a single configuration or load case which

✉ Fugui Xie
xiefg@mail.tsinghua.edu.cn

✉ Xin-Jun Liu
xinjunliu@mail.tsinghua.edu.cn

1 The State Key Laboratory of Tribology and Tsinghua University (DME)-Siemens Joint Research Center for Advanced Robotics, Department of Mechanical Engineering (DME), Tsinghua University, Beijing 100084, China

2 Beijing Key Lab of Precision/Ultra-Precision Manufacturing Equipments and Control, Tsinghua University, Beijing 100084, China

cannot guarantee the validity in the whole workspace. Robust topology optimization (RTO) (Ben-Tal and Nemirovski 1997) and reliability based topology optimization (RBTO) (Kharmanda et al. 2004) are representative methods considering uncertainties. Due to the fact that these two methods require iterative calculation of additional function, the computational efficiency is normally unsatisfactory. In efficient topology optimization of the robotic arm, identifying the worst case is an essential step. For linear structural performance functions, the worst case can be identified using the anti-optimization technique (Lombardi and Haftka 1998). However, the identification of the worst-case is not so straightforward for a nonlinear performance and some effective methods have been proposed (Luo et al. 2009). For the topology optimization of the hybrid robotic arm, taking the kinematic characteristics into consideration is an ideal method to improve efficiency. Therefore, the worst case of each link will be identified based on force analysis to realize global validity within allowable computational time in this paper. On the basis of the identified worst case, the topology optimization can be carried out for each link.

The research on continuum-based topology optimization problem construction started with the pioneering works of homogenization method (Bendsøe and Kikuchi 1988). Sequentially, several representative methods like the evolutionary structural optimization (ESO) method (Xie and Steven 1993), the density-based method (Bendsøe 1989), the level set method (Sethian and Wiegmann 2000) and the independent continuous mapping (ICM) method (Sui et al. 2000) are proposed. Among them, the density-based method is widely used because of its generality and easy implementation. In this method, the integer 0–1 variables are replaced by continuous variables ranging from 0 to 1 to simplify the problem. Proper penalty is normally introduced to eliminate elements with intermediate density values, and the penalty method is often called interpolation scheme. Solid isotropic material with penalization (SIMP) method and rational approximation of material properties (RAMP) method (Stolpe and Svanberg 2001) are two typical interpolation schemes. Besides, meshless density variable approximation methods are frequently used in density-based topology optimization as well (Matsui and Terada 2004). In this paper, the SIMP interpolation method, which is a widely used scheme, will be used to construct the optimization problem. Besides, the objective function construction for links with multiple worst cases is essential for global validity, which requires further investigation in this paper.

Normally, the solving strategy of topology optimization can be summarized into three categories including the optimality criteria (OC) methods (Rozvany and Zhou 1991), the mathematical programming (MP) methods (Bruyneel et al. 2002) and the heuristic methods (Silva Smith 1997). In OC methods, certain criteria or optimal conditions in mathematical programming must be derived. OC methods are widely used in engineering because they are not sensitive to the quantity of variables. However, OC methods demand different criteria for different formulations, which limits its generality in topology optimization. MP methods have been applied in different kinds of optimization problems and has shown many advantages such as high accuracy, wide availability, and etc. In order to improve computational efficiency, the approximation technique and dual method are employed to transform the original optimization problem into a separable convex approximate problem. The methods like SLP (Fujii and Kikuchi 2000), SQP (Sedaghati et al. 2000), SCP (Zillober et al. 2004), CONLIN (Fleury and Braibant 1986) and MMA (Svanberg 1987) are commonly used and representative in the realization of this transformation. In general, heuristic methods include Particle Swarm Optimization (PSO) (Luh and Lin 2011), Genetic Algorithm (GA) (Essiet et al. 2019), Differential Evolution Algorithm (DEA) (Panagant and Bureerat 2018), and etc. Heuristic methods have shown great advantages in optimization with strong nonlinearity, however the convergence to the global optimal solution cannot be guaranteed. The guide-weight method was first proposed in the optimal design of antenna structures (Chen and Ye 1984, 1986). Thereafter, the modified guide-weight method is extended into continuum topology optimization and good results have been obtained (Liu et al. 2014; Xu et al. 2013). As mentioned in Ref. Xu et al. (2013), since the required iteration steps of modified guide-weight is normally far less than representative methods, this method will be used to solve the topology optimization in this paper for fast convergence. Normally, the mesh dependence and checkerboard problem influence the optimal topology greatly and there have been a number of research efforts applied to overcome these problems like variant finite element methods (Diaz and Sigmund 1995), constraint methods (Haber et al. 1996) and filtering techniques (Sigmund 2007). In this work, inspired by sensitivity filtering techniques, a guide-weight filtering method will be proposed to cope with these problems in modified guide-weight method.

The remainder of this paper is organized as follow: In Sect. 2, the workspace with good transmissibility is identified through kinematics analysis. Thereafter, the external forces of each link is analyzed in the workspace. On the basis of force analysis, the effect of axial load and shear is evaluated through the equivalent external load. Sequentially, the worst case is identified efficiently by locating the load case with maximum equivalent external load. In Sect. 3, for links with multiple worst cases, the SIMP interpolation scheme is utilized to construct the optimization problem and the objective function is formulated as the weighted sum of compliance under each worst case. Thereafter, the modified guide-weight method is used to solve the problem and a guide weight filtering method is proposed. Lastly, the CAD model of the hybrid robotic arm is presented based on the derived topology. Section 4 concludes the paper.

2 Worst case identification of the 2-DoF hybrid robotic arm

Topology optimization of the hybrid robotic arm aims to derive the topologies of each link with global validity in the workspace. Therefore, efficiently identifying the worst case in the workspace is an essential step. The computational efficiency of existing worst case identification method is normally unsatisfactory. The worst case identification considering the kinematic characteristics and compliance is a possible method and the computational efficiency is expected to be higher. In this section, the workspace with good transmissibility will be identified first. The effect of shear and axial load will be unified from the aspect of compliance, then the worst case with maximum compliance can be located efficiently.

2.1 Kinematic analysis and workspace identification

The kinematic scheme of the 2-DoF hybrid robotic arm is shown in Fig. 1a. Link *HCE* is shared by parallelogram mechanisms *CFGH* and *ODEC*. *CB* and *CF* are two edges of the triangle link *BFC*. *OABC*, *ODEC* and *CFGH* share a revolute center at point *C*. *OABC* and *ODEC* share a revolute center at point *O*. *OA* is fixed to the base and two coaxial actuating joints are located at point *O*. When *OC* and *OD* are driven, the end-effector can follow an arbitrary curve within the workspace and maintain a definite posture. The angle between *OA* and the *x*-axis is defined as β. δ represents the vertex angle between *CF* and *CB*. The lengths of *OC*, *CE* and *HC* are R_1, L_2 and R_3, respectively. θ_1 is the driven angle between *OC* and the *x*-axis. θ_2 represents the other driven angle between *OD* and the *x*-axis.

The position of the end-effector (denoted by *H*) in coordinate system *O-xy* can be expressed as:

$$\begin{cases} X_{\mathrm{H}} = R_1 \cos\theta_1 + R_3 \cos(\theta_2 + \varphi) \\ Y_{\mathrm{H}} = R_1 \sin\theta_1 + R_3 \sin(\theta_2 + \varphi) \end{cases} \tag{1}$$

Normally, the transmissibility influences the overall performance of the robotic arm greatly. The local transmission index (LTI) is widely used to evaluate the transmissibility, and its definition is:

$$\kappa \;=\; \mathrm{LTI} = \min\left\{\sin\gamma_1, \sin\varepsilon_1, \sin\gamma_2, \sin\varepsilon_2, \sin\gamma_3, \sin\varepsilon_3\right\} \tag{2}$$

The driven angles of the robotic arm are defined as $\theta_1 \in [90°, 180°]$, $\theta_2 \in [0°, 90°]$ to avoid interference and singularity, and the ranges of the driven angles constitute the driving space of the robotic arm. When the driven angles vary in the driving space, all reachable positions of the end-effector constitute the workspace. In this work, the good transmission workspace (GTW) is defined as the area in which the LTI is large than 0.5. Based on the parameter optimization in Ref. Liu et al. (2015), the optimal parameters are derived as: $\beta = 45°$, $\delta = 45°$, $R_1 = 1000\mathrm{mm}$, $R_3 = 1300\mathrm{mm}$, $L_2 = 400\mathrm{mm}$ and $\varphi = 135°$ by considering transmission and workspace requirement. The identified GTW and distribution of LTI are shown in Fig. 1b.

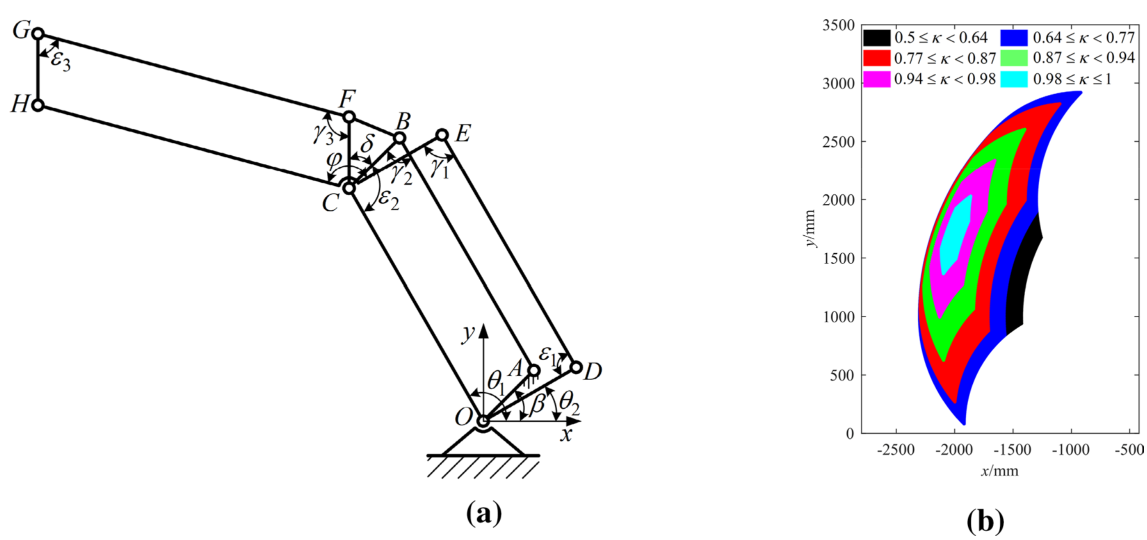

Fig. 1 The 2-DOF hybrid robotic arm: **a** kinematic scheme; **b** GTW and LTI distribution

2.2 Force analysis under external load

The external load $\mathbf{F}_e$ is the payload, and its axis goes along the direction of link *GH*. Under this external load, the internal force of link *GF* can be derived through the equilibrium equation of link *GH*. Specifically, since the axis of the external load goes along the direction of link *GH*, the moment of internal force of link *GF* on joint H should be zero. When robotic arm is in non-singular configuration, the internal force of link *GF* should be zero. Similarly, the internal force of link *AB* can be derived as zero through the equilibrium equation of link *CFB*. Therefore, the internal force of link *CFB* is zero. The force diagrams of links *HCE*, *OC* and *OD* are shown in Fig. 2. For link *HCE*, $\mathbf{F}_{2i}$ denotes the internal force of link *DE*; $\mathbf{F}_{31x}$ and $\mathbf{F}_{31y}$ represent the reaction forces of joint *C* along the *x*- and *y*- axes. The equilibrium equations are derived as shown in Eqs. (3)–(5).

$$\sum \mathbf{F}_x = \mathbf{F}_{2i}\cos\theta_1 - \mathbf{F}_{31x} = 0 \tag{3}$$

$$\sum \mathbf{F}_y = \mathbf{F}_{31y} - \mathbf{F}_{2i}\sin\theta_1 - \mathbf{F}_e = 0 \tag{4}$$

$$\sum \mathbf{M}_C = \mathbf{F}_e R_3\cos(\pi - \varphi - \theta_2) - \mathbf{F}_{2i}L_2\sin\gamma_1 = 0 \tag{5}$$

Similarly, the equilibrium equations of *OC* are shown in Eqs. (6)–(8). $\mathbf{F}_{13x}$ and $\mathbf{F}_{13y}$ are the reaction forces of joint *C* along the *x*- and *y*- axes; $\mathbf{F}_{3x}$ and $\mathbf{F}_{3y}$ denote the reaction forces of joint *O* along the *x*- and *y*- axes; $\mathbf{M}_3$ is the driving torque provided by the actuator.

$$\sum \mathbf{F}_x = \mathbf{F}_{13x} - \mathbf{F}_{3x} = 0 \tag{6}$$

$$\sum \mathbf{F}_y = \mathbf{F}_{3y} - \mathbf{F}_{13y} = 0 \tag{7}$$

$$\sum \mathbf{M}_O = -\mathbf{F}_{13y}R_1\cos\theta_1 - \mathbf{F}_{13x}R_1\sin\theta_1 - \mathbf{M}_3 = 0 \tag{8}$$

The additional equations can be derived as follow:

$$\mathbf{F}_{13x} = \mathbf{F}_{31x},\ \mathbf{F}_{13y} = \mathbf{F}_{31y} \tag{9}$$

The equilibrium equations of link *OD* can be written as:

$$\sum \mathbf{F}_x = \mathbf{F}_{4x} + \mathbf{F}'_{2i}\cos\theta_1 = 0 \tag{10}$$

$$\sum \mathbf{F}_y = \mathbf{F}'_{2i}\sin\theta_1 - \mathbf{F}_{4y} = 0 \tag{11}$$

$$\sum \mathbf{M}_O = \mathbf{F}'_{2i}L_2\sin\varepsilon_1 - \mathbf{M}_4 = 0 \tag{12}$$

where, $\mathbf{F}_{4x}$ and $\mathbf{F}_{4y}$ are the reaction forces of joint *O* in the *x*- and *y*- axes direction; $\mathbf{M}_4$ represents the driving torque provided by the actuator and $\mathbf{F}'_{2i}$ denotes the internal force of link *DE*.

Since the hybrid robotic arm is non-redundant, the forces can be uniquely determined when the configuration and external load are given.

2.3 Worst case identification

For a link under two external loads, the distribution of shear and bending-moment need to be further analyzed. Link *IJK* (Fig. 3a) is under two vertical loads at *I* and *K*, and the beam is in static equilibrium. Then the shear and bending-moment diagrams can be derived as shown in Fig. 3b, c, respectively. The shear and bending-moment diagrams of beams *IJ* and *JK* are the same as that of cantilever beams fixed at joint *J*. As to axial loads, similar results can be obtained as well. Since the joints' positions of the hybrid robotic arm are determined when the location of the end-effector is given. In the following optimization, *HCE* is divided into cantilever beams *HC* and *CE* fixed at point *C*. While *OC* and *OD* are two cantilever beams fixed at point *O*.

For each link, both the magnitude and direction of the external load varies with different configurations. To simplify subsequent calculation, the external loads should be

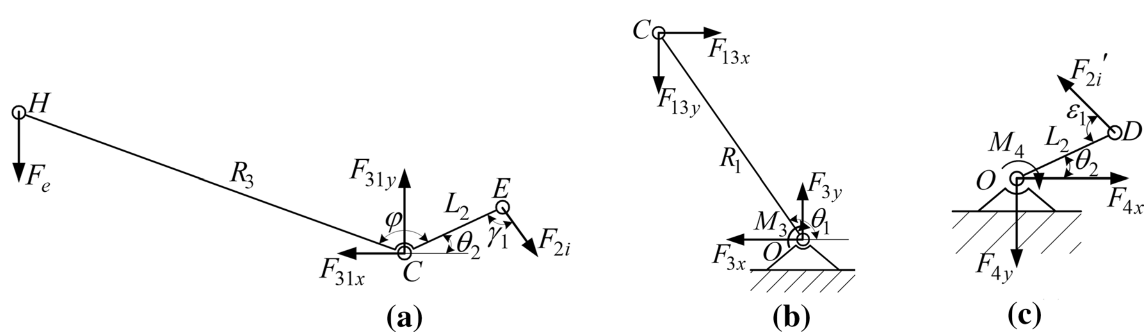

Fig. 2 Force diagram: **a** link HCE; **b** link OC; **c** link OD

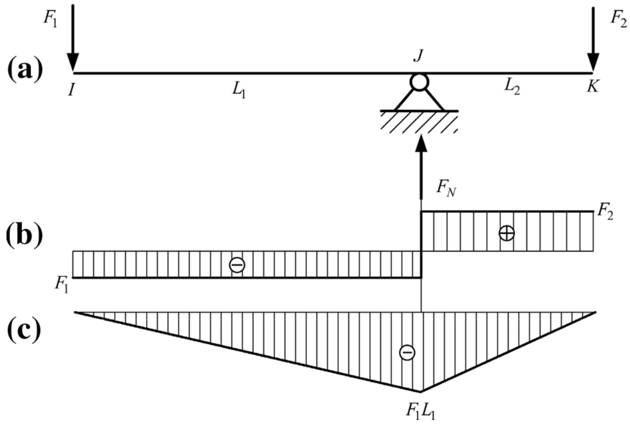

Fig. 3 Analysis of a typical link: **a** force diagram; **b** shear diagram; **c** bending-moment diagram

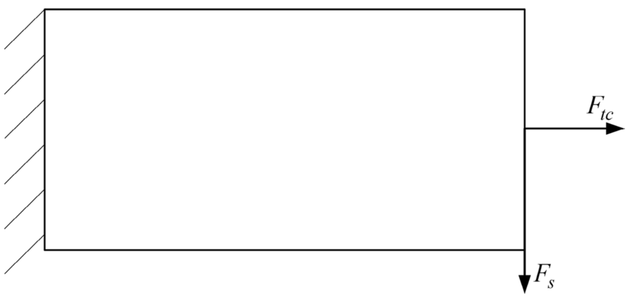

Fig. 4 Load decomposition schematic diagram

decomposed. Due to the fact that the external loads can be regarded as pure concentrated forces acting at the joint, the external loads of each beam can always be decomposed as axial load and shear as shown in Fig. 4.

$\mathbf{F}_{1tc}$ and $\mathbf{F}_{1s}$ represent axial load and shear of beam *HC*; $\mathbf{F}_{2tc}$ and $\mathbf{F}_{2s}$, $\mathbf{F}_{3tc}$ and $\mathbf{F}_{3s}$, $\mathbf{F}_{4tc}$ and $\mathbf{F}_{4s}$ represent axial loads and shears of *CE*, *OC* and *OD*, respectively. The values can be calculated through Eqs. (13)–(16).

$$\mathbf{F}_{1tc} = -\mathbf{F}_e \sin(\varphi + \theta_2),\ \mathbf{F}_{1s} = \mathbf{F}_e \cos(\varphi + \theta_2) \tag{13}$$

$$\mathbf{F}_{2tc} = -\mathbf{F}_{2i} \cos \gamma_1,\ \mathbf{F}_{2s} = \mathbf{F}_{2i} \sin \gamma_1 \tag{14}$$

$$\mathbf{F}_{3tc} = \mathbf{F}_{13x} \cos \theta_1 - \mathbf{F}_{13y} \sin \theta_1,\ \mathbf{F}_{3s} = -\mathbf{F}_{13y} \cos \theta_1 - \mathbf{F}_{13x} \sin \theta_1 \tag{15}$$

$$\mathbf{F}_{4tc} = -\mathbf{F}'_{2i} \cos \varepsilon_1,\ \mathbf{F}_{4s} = \mathbf{F}'_{2i} \sin \varepsilon_1 \tag{16}$$

Normally, a cantilever beam under shear is more fragile. However, when a cantilever beam is under both axial load and shear with changing magnitude, the destructive effect is hard to evaluate perceptually. How to unify the effect of axial load and shear quantitatively is the key to identify the worst cases of each beam. In general, the strain energy can be used to evaluate the closeness to structure failure. In topology optimization, the compliance, which characterizes the internal strain energy, is often used as the objective function to be minimized. Thus, evaluating the effect of axial load and shear from the aspect of compliance is an ideal choice. In topology optimization, the structural compliance is defined as:

$$C = \mathbf{F}^{\mathrm{T}}\mathbf{U} = \mathbf{U}^{\mathrm{T}}\mathbf{K}\mathbf{U} \tag{17}$$

where $\mathbf{F}$ is the external load, $\mathbf{U}$ is the displacement vector and $\mathbf{K}$ is the stiffness matrix.

For a cantilever beam (Fig. 4) with both axial load and shear, under the assumption of small elastic deformation, the compliance C can be expressed as:

$$C = (\mathbf{F}_{tc} + \mathbf{F}_s)^{\mathrm{T}}(\mathbf{U}_{tc} + \mathbf{U}_s) = \mathbf{F}_{tc}^{\mathrm{T}}\mathbf{U}_{tc} + \mathbf{F}_s^{\mathrm{T}}\mathbf{U}_s = C_{tc} + C_s \tag{18}$$

where, C_s is the compliance when only shear is applied; while C_{tc} represents compliance under pure axial load. Therefore, the compliance of the cantilever beam is the sum of compliance caused by axial load and shear. Based on Eq. (17), the following equation can be derived:

$$C = \mathbf{F}^{\mathrm{T}}\mathbf{U} = \mathbf{F}^{\mathrm{T}}\mathbf{K}^{-1}\mathbf{F} \tag{19}$$

Therefore, the compliance under pure axial load or shear can be derived as follow:

$$C_{tc} = \eta_1 \mathbf{F}_{tc}^2,\ C_s = \eta_2 \mathbf{F}_s^2 \tag{20}$$

In Eq. (21), C_{s-s} and C_{tc-s} represent compliance under pure shear or axial load with the same magnitude, respectively and η is defined as the equivalent coefficient of axial load with respect to shear.

$$\eta = \sqrt{C_{tc-s}/C_{s-s}},\ \|\mathbf{F}_{tc-s}\| = \|\mathbf{F}_{s-s}\| \tag{21}$$

Based on Eqs. (17)–(21), the relation between compliance and external load can be expressed as:

$$\begin{aligned} C &= \eta_1 \mathbf{F}_s^2 + \eta_2 \mathbf{F}_{tc}^2 = \eta_1 (\mathbf{F}_s^2 + \frac{\eta_2}{\eta_1}\mathbf{F}_{tc}^2) \\ &= \eta_1 (\mathbf{F}_s^2 + \eta^2 \mathbf{F}_{tc}^2) = \eta_1 (\mathbf{F}_s + \eta \mathbf{F}_{tc})^{\mathrm{T}} (\mathbf{F}_s + \eta \mathbf{F}_{tc}) \end{aligned} \tag{22}$$

To evaluate the overall effect of external load, the equivalent external load is defined as:

$$F_{\mathrm{eq}} = \|\mathbf{F}_s + \eta \mathbf{F}_{tc}\| \tag{23}$$

The worst cases of each link are identified by locating the maximum equivalent external load. The computational efficiency is higher because iterative calculation is avoided. The identification can be expanding into three-dimension by calculating the equivalent coefficient of moments as well.

In this situation, the dimension of equivalent coefficient of moment with respect to force is reciprocal to length. In finite element analysis (FEA), the compliance can be calculated through Eq. (24). $\mathbf{u}_i$ represents the displacement vector of the ith element; $\mathbf{k}_i$ is the stiffness matrix of the ith element and N is the number of elements.

$$C = \mathbf{U}^{\mathrm{T}}\mathbf{K}\mathbf{U} = \sum_{i=1}^{N} \mathbf{u}_i^{\mathrm{T}}\mathbf{k}_i\mathbf{u}_i \tag{24}$$

Since the hybrid robotic arm is developed based on a planar mechanism, the topology optimization will be carried out as a 2D problem. Based on the parameters of each link, the design domain of beam HC is determined as a 1300 mm × 200 mm rectangle, which is discreted into 130 × 20 elements; the design domain of beams CE and OD are 400 mm × 200 mm rectangles, which is discreted into 40 × 20 elements; and the design domain of beam OC is determined as a 1000 mm × 300 mm rectangle, which is discreted into 100 × 30 elements. The external load is applied to cantilever beams at the center of the right boundary line, and the left boundary is constrained. The derived equivalent coefficients of each beam are listed in Table 1. A smaller coefficient indicates that the beam is more sensitive to shear. It is shown that a slender cantilever beam (like HC) possess smaller coefficient, which is consistent with the principal of mechanics as well.

When the external load $\mathbf{F}_e = 2000\mathrm{N}$, the equivalent external load distribution in the driving space is shown in Fig. 5, and the equivalent load distribution is plotted in task workspace as well (Fig. 6). Based on the distribution, the locations and the external loads of the identified worst cases are listed in Table 2. The equivalent external load distribution of beam OD is the same as that of beam CE. Therefore, the optimal topology of beam OD should be the same as that of beam CE as well.

Table 1 Equivalent coefficients of each beam

Results	Beam *HC*	Beam *CE*	Beam *OC*	Beam *OD*
Compliance (axial load)	0.0042	0.0020	0.0027	0.0020
Compliance (shear)	0.5415	0.0190	0.0773	0.0190
Equivalent coefficient η	0.088	0.325	0.187	0.325

3 Topology optimization under the worst case

Since the worst cases of each link are identified, how to construct and solve the topology optimization is the main challenge encountered. In the formulation of the optimization problem, all worst cases should be taken into consideration for global validity, and the solving process is expected to converge as quickly as possible. In topology optimization, the mesh dependence and checkerboard problem are non-negligible problems as well. The methods to solve the aforementioned problems will be presented in this section.

3.1 Topology optimization problem and guide weight filtering method

The topology optimization of minimum compliance under a certain weight constraint can be expressed as:

$$\begin{cases} \text{find}: \ \boldsymbol{\rho} = [\rho_1, \rho_2, \cdots, \rho_N]^{\mathrm{T}} \in R^N \\ \text{min}: \ C(\boldsymbol{\rho}) \\ \text{s.t.}\, M \le fM_0 \\ 0 < \rho_{\min} \le \rho_i \le 1 \quad i = 1, 2, \cdots N \end{cases} \tag{25}$$

In the density-based method, the design variable ρ_i is the relative density of the ith element in FEA; $\rho_{\min}$ is the minimum value of the design variables to avoid singularity; N is the quantity of the elements; C is the structural compliance; M and M_0 represent the actual and initial weight of the structure, respectively; f is the weight fraction. Based on the SIMP method, the following equation can be derived.

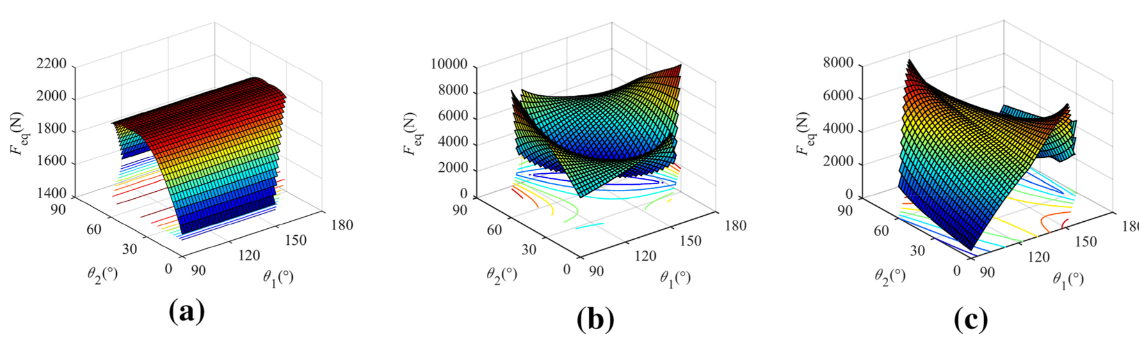

Fig. 5 Equivalent external load distribution atlases: **a** beam *HC*; **b** beams *CE* and *OD*; **c** beam *OC*

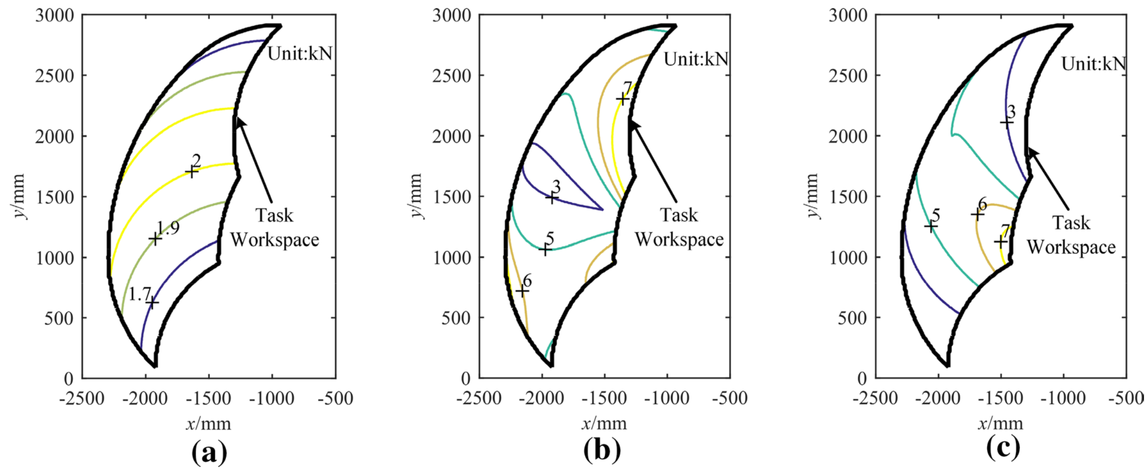

Fig. 6 Equivalent load distribution in task workspace: **a** beam *HC*; **b** beams *CE* and *OD*; **c** beam *OC*

Table 2 Worst case of the hybrid robotic arm

Results		Beam *HC*		Beam *CE* and *OD*		Beam *OC*
Worst case location	θ_1	(90°, 180°)	(90°, 180°)	90°	180°	116.4°
	θ_2	40°	50°	60°	30°	86.4°
External loads	Axial load	– 174.3 N	174.3 N	– 10875 N	10875 N	– 4104.3 N
	Shear	– 1992.4 N	– 1992.4 N	– 6278.5 N	– 6278.5 N	6878.N

$$\mathbf{k}_i = \rho_i^p \mathbf{k}_{io} \tag{26}$$

where p is the penalty factor; $\mathbf{k}_i$ and $\mathbf{k}_{io}$ are the actual and initial stiffness matrices of the ith element, respectively. Substituting Eq. (26) into Eq. (24), it leads to:

$$C = \sum_{i=1}^{N} \rho_i^p \mathbf{u}_i^{\mathrm{T}} \mathbf{k}_{io} \mathbf{u}_i \tag{27}$$

From Eq. (27), we can get

$$\frac{\partial C}{\partial \rho_i} = \mathbf{F}^{\mathrm{T}} \frac{\partial \mathbf{U}}{\partial \rho_i} + \left(\frac{\partial \mathbf{F}}{\partial \rho_i} \right)^{\mathrm{T}} \mathbf{U} \tag{28}$$

Based on $\mathbf{F} = \mathbf{KU}$, it leads to:

$$\frac{\partial \mathbf{F}}{\partial \rho_i} = \mathbf{K} \frac{\partial \mathbf{U}}{\partial \rho_i} + \frac{\partial \mathbf{K}}{\partial \rho_i} \mathbf{U} \tag{29}$$

The derivative of the nodal displacement vector $\mathbf{U}$ can be expressed as:

$$\frac{\partial \mathbf{U}}{\partial \rho_i} = \mathbf{K}^{-1} \left(\frac{\partial \mathbf{F}}{\partial \rho_i} - \frac{\partial \mathbf{K}}{\partial \rho_i} \mathbf{U} \right) \tag{30}$$

Substituting Eq. (30) into Eq. (28),

$$\frac{\partial C}{\partial \rho_i} = 2 \frac{\partial \mathbf{F}}{\partial \rho_i} \mathbf{U}^{\mathrm{T}} - \mathbf{U}^{\mathrm{T}} \frac{\partial \mathbf{K}}{\partial \rho_i} \mathbf{U} \tag{31}$$

Neglecting the variation of load vector $\boldsymbol{F}$, the formula can be derived as:

$$\frac{\partial C}{\partial \rho_i} = -\sum_{j=1}^{N} \mathbf{u}_j^{\mathrm{T}} \frac{\partial \mathbf{k}_j}{\partial \rho_i} \mathbf{u}_j = -p \rho_i^{p-1} \mathbf{u}_i^{\mathrm{T}} \mathbf{k}_{io} \mathbf{u}_i \tag{32}$$

The weight of the design domain can be derived as:

$$M = \sum_{i=1}^{N} \rho_i \rho_m v_i \tag{33}$$

where v_i is the volume of the ith element and ρ_m is the density of the material. Then

$$\frac{\partial M}{\partial \rho_i} = \rho_m v_i \tag{34}$$

According to the modified guide-weight method (Liu et al. 2011), the proportional weight H_i, the generalized weight W_i, the guide weight G_i and the total guide weight G can be derived as follow:

$$\begin{cases} H_i = \frac{\partial M}{\partial \rho_i} = \rho_m v_i \\ W_i = \rho_i H_i = \rho_i \rho_m v_i \\ G_i = -\rho_i \frac{\partial C}{\partial \rho_i} = p \rho_i^p \mathbf{u}_i^T \mathbf{k}_{io} \mathbf{u}_i \\ G = \sum_{i=1}^{N} G_i = \sum_{i=1}^{N} p \rho_i^p \mathbf{u}_i^T \mathbf{k}_{io} \mathbf{u}_i = pC \end{cases} \tag{35}$$

The iterative formula can be written as:

$$x_i^{(k+1)} = \begin{cases} 1 \text{ if } \rho_i \geq 1 \\ \alpha \left(\frac{p \rho_i^p \mathbf{u}_i^T \mathbf{k}_{io} \mathbf{u}_i}{\lambda \rho_m v_i} \right)^{(k)} + (1-\alpha) \rho_i^{(k)} \text{ if } \rho_{\min} < \rho_i < 1 \quad i = 1, 2, \cdots N \\ \rho_{\min} \text{ if } \rho_i \leq \rho_{\min} \end{cases} \tag{36}$$

The Lagrange multiplier can be derived as:

$$\lambda = \frac{pC}{fM_0} \tag{37}$$

There are more than one worst case for beams HC, CE and OD (as shown in Table2). If the objective function only considers one worst case, the derived topology can be fragile under other worst cases. In this paper, objective function is formulated as the weighted sum of compliance under each worst case to cope with the topology optimization under multiple worst cases. The optimization problem can be written as:

$$\begin{cases} \text{find}: \ \boldsymbol{\rho} = [\rho_1, \rho_2, \cdots, \rho_N]^{\mathrm{T}} \in R^N \\ \min: \ C_{\text{sum}}(\boldsymbol{\rho}) = \sum_{j=1}^{S} w_j C_j(\boldsymbol{\rho}) \\ \text{s.t.} \ M \leq fM_0 \\ 0 < \rho_{\min} \leq \rho_i \leq 1 \quad i = 1, 2, \cdots N \end{cases} \tag{38}$$

where S is the number of worst cases; w_j is the weight coefficient of the jth worst case; C_j is the compliance under the jth worst case.

Then, the following formula can be derived:

$$\frac{\partial C_{\text{sum}}}{\partial \rho_i} = -p\rho^{p-1} \sum_{j=1}^{S} w_j \mathbf{u}_{ij}^{\mathrm{T}} \mathbf{k}_{io} \mathbf{u}_{ij} \tag{39}$$

where $\mathbf{u}_{ij}$ is the displacement vector of the ith element under the jth load case. For beams HC, CE and OD, $S = 2$ and $w_j = 0.5$ considering the probability of occurrence of each worst case.

The guide weight, the total guide weight and the Lagrange multiplier can be derived as:

$$G_i = -\rho_i \frac{\partial C_{\text{sum}}}{\partial \rho_i} = p \sum_{j=1}^{S} w_j \rho_i^p \mathbf{u}_{ij}^{\mathrm{T}} \mathbf{k}_{io} \mathbf{u}_{ij} \tag{40}$$

$$G = \sum_{i=1}^{N} G_i = p \sum_{i=1}^{N} \sum_{j=1}^{S} w_j \rho_i^p \mathbf{u}_{ij}^{\mathrm{T}} \mathbf{k}_{io} \mathbf{u}_{ij} = pC_{\text{sum}} \tag{41}$$

$$\lambda = \frac{pC_{sum}}{fM_0} \tag{42}$$

In optimization, the mesh dependency and checkerboard problem will deteriorate the optimal topology. To address these non-negligible problems, a guide weight filtering method is proposed. This method modifies the guide weight of an element based on the guide weight in a fixed neighborhood.

This filtering formula of the ith element can be derived as:

$$\hat{G}_i = \frac{1}{\rho_k \sum_{i=1}^{N} \hat{L}_i} \sum_{i=1}^{N} \hat{L}_i \rho_i G_i \tag{43}$$

where N is the total number of elements in FEA. The convolution operator $\hat{L}_i$ is written as:

$$\hat{L}_i = r_{\min} - \text{dist}(k, i), \ \left\{ i \in N | \text{dist}(k, i) \leq r_{\min} \right\}, \quad k = 1, \ldots N \tag{44}$$

The operator $\text{dist}(k, i)$ is defined as the distance between the center of element k and the center of element i. The convolution operator $\hat{L}_i$ is zero outside the filter area. In the design variables updating process, the value of $\hat{G}_i$ will replace the value of G_i. In this method, the guide weight of an element is modified as the weighted average guide weight in the neighborhood. Through this filtering method, the mesh dependency and checkerboard problem can be eliminated.

3.2 Optimization of the 2-DoF hybrid robotic arm

In this section, the topology optimization of each link is carried out in MATLAB environment and the optimization procedure is shown in Fig. 7. The worst case will be identified first by searching the maximum equivalent external loads of each link in the workspace. Thereafter, the design variables will be optimized based on the iterative criterion presented in Sect. 3.1 and the structure will be updated.

All necessary parameters in topology optimization are listed in Table 3. The post process is executed when convergence is reached.

The iteration processes and the final results of three cantilever beams are shown in Figs. 7, 8, 9. As shown in Fig. 8, the optimization procedure of beam HC converges within 60 steps and the final topology has a clear boundary.

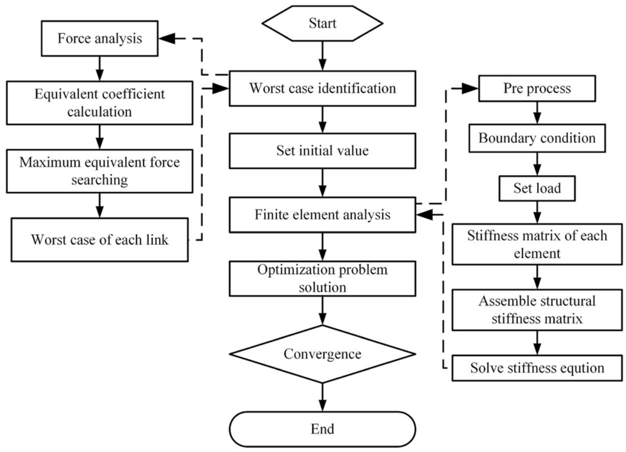

Fig. 7 Flowchart of topology optimization procedure

Table 3 Parameters for topology optimization

Parameters	Value	Meaning
E	2.06×10^{11}	Young's modules
μ	0.3	Poisson's ratio
p	4	Penalty factor
α	0.4	Step factor
f	0.3	Weight fraction
$\boldsymbol{\rho}_0$	[1,1,…,1]	Initial values of the design variables

As shown in Figs. 9 and 10, the optimal topology of beams *CE* and *OC* can be derived within 40 steps, which proves the fast convergence of modified guide-weight method.

3.3 Performance comparison

Based on the derived topologies of each beam, the CAD model of the optimized hybrid robotic arm is shown in Fig. 11a. To validate the effect of the topology optimization, the performance comparison is carried out based on finite element analysis. To make the comparison unbiased, the weight and shape of the baseline robotic arm is the same with the optimized one and the CAD model is shown in Fig. 11b.

The vertical stiffness and natural frequencies under three typical configurations are compared using ANSYS 15.0 Workbench. The simulation results are listed in Table 4 and the selected configurations are shown in Fig. 12. The three configurations correspond to the end-effector location at the lower, higher and middle part of the task workspace. The vertical stiffness refers to the stiffness of the end-effector along the vertical direction. Based on the simulation result, the vertical stiffness of the optimized robotic arm can achieve two times of that of the baseline one. Besides, the first natural frequency can be improved more than 50% after the optimization. Therefore, the optimization method proposed in this paper is an effective way to improve the performance of the robotic arm.

4 Conclusion

In this paper, the topology optimization of the 2-DoF hybrid robotic arm is accomplished based on efficient worst case identification. On the basis of forward and inverse kinematics analysis, the good transmission workspace is identified under the constraint of LTI. By analyzing the external forces of each link in the workspace, the equivalent external load is proposed to evaluate the effect of axial load and shear from the aspect of compliance. By searching for the maximum equivalent external load, the worst case with maximum compliance in the workspace is efficiently identified. Since the identification requires no iterative calculation, the computational efficiency is expected to be higher. Thereafter, the SIMP interpolation scheme is used to construct the optimization problem. By formulating the objective function as the weighted sum of compliance under each worst

Fig. 8 Topology optimization of beam *HC*: **a** iteration process; **b** optimal topology

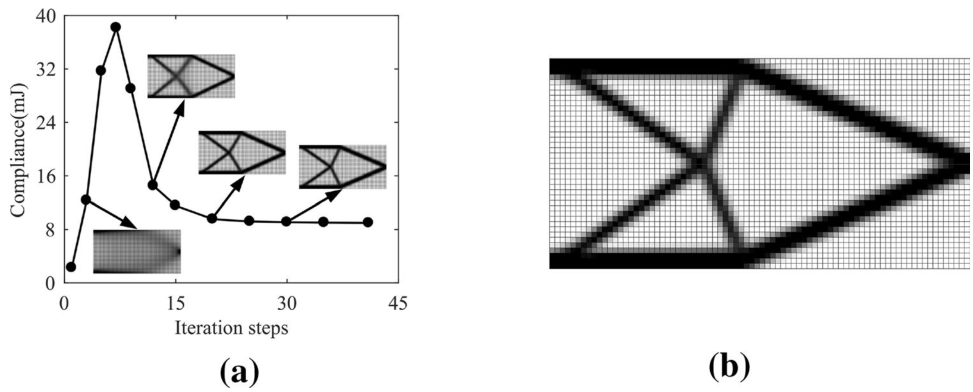

Fig. 9 Topology optimization of beam *CE*: **a** iteration process; **b** optimal topology

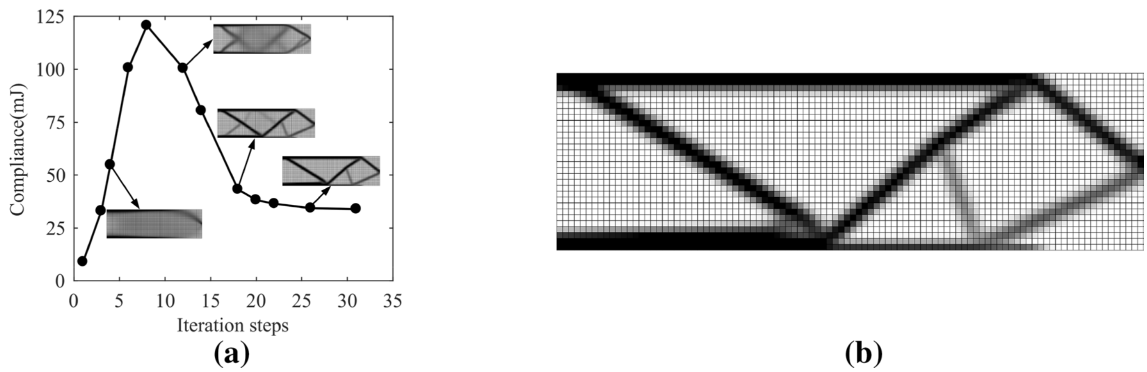

Fig. 10 Topology optimization of beam *OC*: **a** iteration process; **b** optimal topology

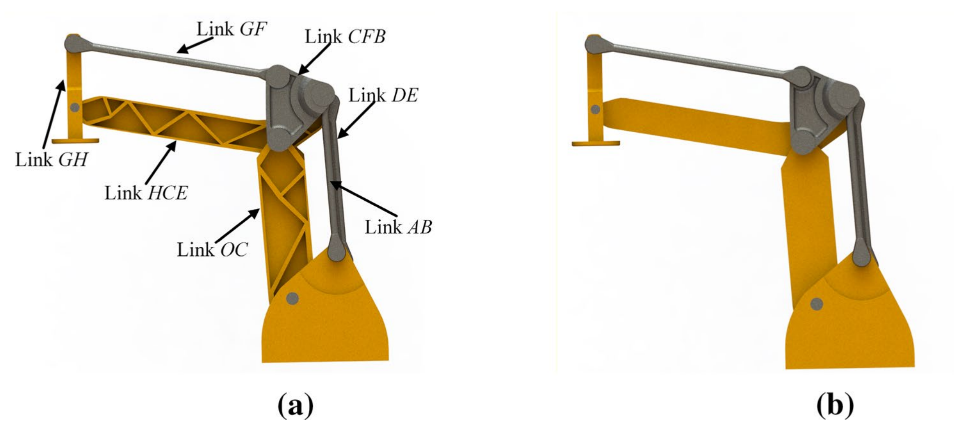

Fig. 11 CAD model of the robotic arm: **a** the optimized one; **b** the baseline one

case, global validity can be further improved. For fast convergence, the modified guide-weight method is utilized as the iterative criterion and a guide weight filtering method is proposed to eliminate the mesh dependence and checkerboard problem. Based on the derived optimal topology, the CAD model of the hybrid robotic arm is presented. The effect of the optimization method has been testified through performance comparison between the optimized robotic arm and the baseline one based on finite element analysis. The derived CAD model is very helpful to the development of the 2-DoF robotic arm and the optimization approach can be further applied to other hybrid robotic arms as well.

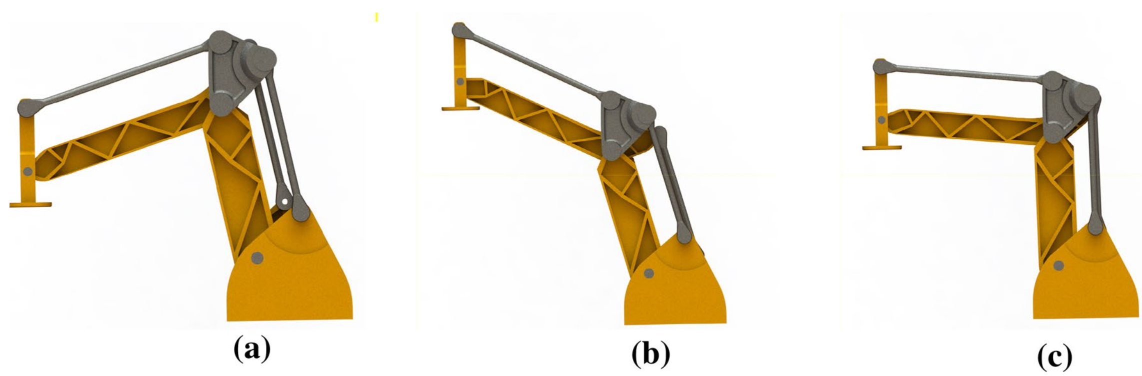

Fig. 12 Selected typical configurations: **a** Configuration I; **b** Configuration II; **c** Configuration III

Table 4 the performance comparison of two robotic arms

		Configuration I	Configuration II	Configuration III
Baseline	Vertical stiffness (N/μm)	4.33	3.93	4.15
	1st natural frequency (Hz)	8.01	8.52	7.64
Optimized	Vertical stiffness (N/μm)	10.78	10.17	10.15
	1st natural frequency(Hz)	13.22	14.63	12.68

Acknowledgements This work is supported by the National Key Scientific and Technological Project of China under Grant No. 2018ZX04018001, National Natural Science Foundation of China under Grant No. 91948301, and Beijing Municipal Science and Technology Commission under Grant No. Z181100003118003.

References

Bendsøe, M.P.: Optimal shape design as a material distribution problem. Struct. Optim. **1**(4), 193–202 (1989)

Bendsøe, M.P., Kikuchi, N.: Generating optimal topologies in structural design using a homogenization method. Comput. Methods Appl. Mech. Eng. **71**(2), 197–224 (1988)

Ben-Tal, A., Nemirovski, A.: Robust truss topology design via semidefinite programming. SIAM J. Optim. **7**(4), 991–1016 (1997)

Bi, W.Y., Xie, F.G., Liu, X.J., Luo, X.: Optimal design of a novel 4-degree-of-freedom parallel mechanism with flexible orientation capability. Proc. Inst. Mech. Eng. Part B J. Eng. Manuf. **233**(2), 632–642 (2019)

Bruyneel, M., Duysinx, P., Fleury, C.: A family of MMA approximations for structural optimization. Struct. Multidiscip. Optim. **24**(4), 263–276 (2002)

Chen, S. X., Ye, S. H.: Criterion method for the optimal design of antenna structure. Acta Mech. Sol. Sinica **5**(4), 482–498 (1984)

Chen, S.X., Ye, S.H.: A guide-weight criterion method for the optimal design of antenna structures. Eng. Optim. **10**(3), 199–216 (1986)

Chen X., Liu X. J., & Xie F. G.: Screw theory based singularity analysis of Lower-Mobility parallel robots considering the Motion/Force transmissibility and constrainability. Math. Prob. Eng. **2015**, 487956 (2015)

Da Silva Smith, O.: Topology optimization of trusses with local stability constraints and multiple loading conditions—a heuristic approach. Struct. Optim. **13**(2–3), 155–166 (1997)

Diaz, A., Sigmund, O.: Checkerboard patterns in layout optimization. Struct. Optim **10**(1), 40–45 (1995)

Essiet, I.O., Sun, Y., Wang, Z.: Improved genetic algorithm based on particle swarm optimization-inspired reference point placement. Eng. Optim. **51**(7), 1097–1114 (2019)

Fleury, C., Braibant, V.: Structural optimization: a new dual method using mixed variables. Int. J. Numer. Meth. Eng. **23**(3), 409–428 (1986)

Fujii, D., Kikuchi, N.: Improvement of numerical instabilities in topology optimization using the SLP method. Struct. Multidiscip. Optim. **19**(2), 113–121 (2000)

Haber, R.B., Jog, C.S., Bendsøe, M.P.: A new approach to variable-topology shape design using a constraint on perimeter. Struct. Optim **11**(1–2), 1–12 (1996)

Jin, X., Li, G.X., Zhang, M.: Design and optimization of nonuniform cellular structures. Proc. Inst. Mech. Eng. Part C J. Mech. Eng. Sci. **232**(7), 1280–1293 (2018)

Kharmanda, G., Olhoff, N., Mohamed, A., Lemaire, M.: Reliability-based topology optimization. Struct. Multidiscip Optim. **26**(5), 295–307 (2004)

Liu, X.J., Li, Z.D., Chen, X.: A new solution for topology optimization problems with multiple loads: the guide-weight method. Sci. China Technol. Sci. **54**(6), 1505–1514 (2011)

Liu, X.J., Wang, C., Zhou, Y.H.: Topology optimization of thermoelastic structures using the guide-weight method. Sci. China Technol. Sci. **57**(5), 968–979 (2014)

Liu, X.J., Li, J., Zhou, Y.H.: Kinematic optimal design of a 2-degree-of-freedom 3-parallelogram planar parallel manipulator. Mech. Mach. Theory **87**, 1–17 (2015)

Lombardi, M., Haftka, R.T.: Anti-optimization technique for structural design under load uncertainties. Comput. Methods Appl. Mech. Eng. **157**(1–2), 19–31 (1998)

Luh, G.C., Lin, C.Y.: Optimal design of truss-structures using particle swarm optimization. Comput. Struct. **89**(23–24), 2221–2232 (2011)

Luo, Y., Kang, Z., Luo, Z., Li, A.: Continuum topology optimization with non-probabilistic reliability constraints based on multi-ellipsoid convex model. Struct. Multidiscip. Optim. **39**(3), 297–310 (2009)

Luo, X., Xie, F.G., Liu, X.J., Li, J.: Error modeling and sensitivity analysis of a novel 5-degree-of-freedom parallel kinematic machine tool. Proc. Inst. Mech. Eng. Part B J. Eng. Manuf. **233**(6), 1637–1652 (2019)
Matsui, K., Terada, K.: Continuous approximation of material distribution for topology optimization. Int. J. Numer. Meth. Eng. **59**(14), 1925–1944 (2004)
Panagant, N., Bureerat, S.: Truss topology, shape and sizing optimization by fully stressed design based on hybrid grey wolf optimization and adaptive differential evolution. Eng. Optim. **50**(10), 1645–1661 (2018)
Rozvany, G.I.N., Zhou, M.: The COC algorithm, part I: cross-section optimization or sizing. Comput. Methods Appl. Mech. Eng. **89**(1–3), 281–308 (1991)
Sedaghati, R., Tabarrok, B., Suleman, A., Dost, S.: Optimization of adaptive truss structures using the finite element force method based on complementary energy. Trans. Can. Soc. Mech. Eng. **24**(1B), 263–271 (2000)
Sethian, J.A., Wiegmann, A.: Structural boundary design via level set and immersed interface methods. J. Comput. Phys. **163**(2), 489–528 (2000)
Sigmund, O.: Morphology-based black and white filters for topology optimization. Struct. Multidiscip. Optim. **33**(4–5), 401–424 (2007)
Smyl, D.: An inverse method for optimizing elastic properties considering multiple loading conditions and displacement criteria. J. Mech. Des. **140**(11), 111411 (2018)
Stolpe, M., Svanberg, K.: An alternative interpolation scheme for minimum compliance topology optimization. Struct. Multidiscip. Optim. **22**(2), 116–124 (2001)
Sui, Y.K., Yang, D.Q., Sun, H.C.: Uniform ICM theory and method on optimization of structural topology for skeleton and continuum structures. Chin. J. Comput. Mech. **17**(1), 28–33 (2000)
Svanberg, K.: The method of moving asymptotes—a new method for structural optimization. Int. J. Numer. Meth. Eng. **24**(2), 359–373 (1987)
Wang, X., Zhang, D., Zhao, C., Zhang, P., Zhang, Y., Cai, Y.: Optimal design of lightweight serial robots by integrating topology optimization and parametric system optimization. Mech. Mach. Theory **132**, 48–65 (2019)
Xie, Y.M., Steven, G.P.: A simple evolutionary procedure for structural optimization. Comput. Struct. **49**(5), 885–896 (1993)
Xie, F.G., Liu, X.J., Wu, C., Zhang, P.: A novel spray painting robotic device for the coating process in automotive industry. Proc. Inst. Mech. Eng. Part C J. Mech. Eng. Sci. **229**(11), 2081–2093 (2015)
Xu, H.Y., Guan, L.W., Chen, X., Wang, L.P.: Guide-weight method for topology optimization of continuum structures including body forces. Finite Elem. Anal. Des. **75**, 38–49 (2013)
Zillober, C., Schittkowski, K., Moritzen, K.: Very large scale optimization by sequential convex programming. Optim. Methods Softw **19**(1), 103–120 (2004)

Publisher's Note Springer Nature remains neutral with regard to jurisdictional claims in published maps and institutional affiliations.

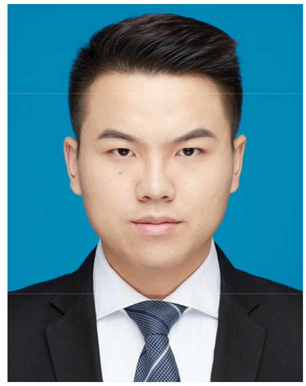

Zenghui Chong received the B.S. degree in Aircraft Manufacturing Engineering from Northwestern Polytechnical University, China, in 2017. He is currently working toward the Ph.D. degree with the Department of Mechanical Engineering, Tsinghua University, Beijing, China. His research interests include the design, dynamics and control of parallel/hybrid robots.

Fugui Xie received the B.S. degree in Mechanical Engineering from Tongji University, China, in 2005, and the Ph.D. degree in Mechanical Engineering from Tsinghua University, China, in 2012. He is currently an Associate Professor with the Department of Mechanical Engineering, Tsinghua University, Beijing, China. From 2012 to 2014, he worked as a Postdoctoral Researcher at Tsinghua University. He was an Alexander von Humboldt (AvH) Research Fellow at Fraunhofer Institute for Machine Tools and Forming Technology (IWU) in Germany in 2016. His research interests include parallel robotic mechanisms, high-speed parallel robots and mobile machining robots.

Xin-Jun Liu received the B.S. and M.S. degrees in Mechanical Design and Manufacturing from Northeast Heavy Machinery Institute, Qinhuangdao, China, in 1994 and 1996, respectively, and the Ph.D. degree in Mechanical Engineering from Yanshan University, Qinhuangdao, China, in 1999. He is currently a Professor with the Department of Mechanical Engineering, Tsinghua University, China. From 2000 to 2001, he was a Postdoctoral Researcher at Tsinghua University. He was an Alexander von Humboldt (AvH) Research Fellow at the University of Stuttgart, Germany from 2004 to 2005. His research interests include robotics, parallel mechanisms, parallel kinematic machines and advanced manufacturing equipment.

Jinsong Wang received the B.S., M.S. and Ph.D. degree in Mechanical Engineering from Tsinghua University in 1986, 1988 and 1991, respectively. He is currently a Professor with the Department of Mechanical Engineering, Tsinghua University, Beijing, China. His research interests include advanced manufacturing technology and equipment, electronics manufacturing technology and equipment, robotics and green manufacturing.

Peng Li received the B.S. degree in Mechanical Engineering from Zhengzhou University, China, in 2013, and the M.S. degree in Mechanical Engineering from University of Chinese Academy of Sciences, China, in 2017. He is currently working toward the Ph.D. degree with the Department of Mechanical Engineering, Tsinghua University, Beijing, China. His current research interests include the design and application of collaborative robots.